Pore Size Measurement in Core Plugs with Magnetic Resonance based on Brownstein-Tarr Relaxation Theory

Peiyuan Yan[1], *Florin* Marica[1], *Benjamin* Nicot[2], *Derrick* Green[3], and *Bruce J.* Balcom[1*]

[1]UNB MRI Centre, Department of Physics, University of New Brunswick, Fredericton, New Brunswick, Canada
[2]TotalEnergies, Avenue Larribau, 64000 Pau, France
[3]Green Imaging Technologies, 520 Brookside Drive, Fredericton, New Brunswick, E3A 8V2, Canada

Abstract. The fast diffusion regime of Brownstein-Tarr theory is commonly employed to interpret MR signal lifetime distributions in terms of the pore size distribution. The intermediate regime of Brownstein-Tarr theory, which we and others believe is commonly encountered in rock core systems, is more complicated and diffusion to the pore surface influences the observed relaxation time distributions. In this work, we introduce glass microcapillaries to experimentally explore the intermediate regime. We employ Brownstein-Tarr theory in the intermediate regime to estimate the dominant pore size and surface relaxivities of a series of sandstone core plugs. Modest changes in the sample temperature shifts the Brownstein-Tarr number and permits a non-linear fitting of the ground mode peak lifetime shift to permit these estimations. Knowledge of the surface relaxivity and non-ground mode behaviour permits the T_2 distribution to be converted to a pore size distribution.

1 Introduction

It is widely recognized that enhanced magnetic resonance (MR) relaxation of fluids within porous media occurs due to surface relaxation [1]. Fluid molecules diffuse to, and relax, on or near the pore surface. This process is influenced by variables such as the size and shape of the pores, the presence of paramagnetic substances on the pore surface, and the diffusivity of the fluid [2]. The application of surface relaxation for estimating pore size stems from the pioneering work of Brownstein and Tarr [3]. The method commonly employed establishes a direct correlation between relaxation time and pore size, founded on the assumption that the fluid relaxation occurs within the fast diffusion regime of Brownstein-Tarr (BT) theory [4, 5]. However, if the fluid relaxation occurs outside of the fast diffusion regime, a direct pore size measurement is problematic since the observed relaxation times also depend on fluid diffusion to the pore surface.

Following the work of Bloch and Torrey [6], Brownstein and Tarr [3] successfully interpreted multi-exponential MR decay in unimodal pore systems. They accomplished this by defining three diffusion regimes, fast, intermediate, and slow, based on the BT number. The BT number is a unitless quantity that relates the pore size, surface relaxivity, and fluid self-diffusion coefficient. The MR behavior distinctly varies depending on whether the fluid relaxation occurs in the fast diffusion or the intermediate regime. Specifically, within an individual pore, the MR signal displays a multi-exponential behavior in the intermediate regime, while it displays a single exponential decay in the fast diffusion regime. Brownstein and Tarr successfully solved the Bloch-Torrey equation, categorizing the solutions into zero mode (also called the ground mode) and non-zero modes (or non-ground modes). In the fast diffusion regime, the ground mode dominates, and the non-ground modes are undetectable. The multi-exponential MR decay observed experimentally in such a case results from a distribution of pore sizes. However, in the intermediate regime, while the ground mode still dominates, there is an increase in the amplitudes of non-ground modes. The non-ground modes from larger pores may contribute to the MR signal at short lifetime, which, under the fast diffusion assumption, would be considered as originating from smaller pores. An accurate estimation of surface relaxivity can help mitigate this overlap by calculating the distribution of non-ground mode relaxation times [7].

The characteristic feature of the intermediate regime is the detection of short lifetime signals originating from the so-called non-ground modes of relaxation. In this work, we consider the basics of BT theory, with a specific focus on the intermediate regime. We employed a model glass microcapillary system to validate BT theory. One major difficulty with BT theory applied to porous media has been the lack of a well characterized model system. By altering the size of the pore space in a series of glass microslides, we observed shifts in both diffusion regime and relaxation time, which are in accordance with the predictions of BT theory. The intermediate regime was employed to interpret measurements of sandstone core plugs, which we will detail further in this paper.

* Corresponding author: bjb@unb.ca

BT theory has previously been utilized to estimate the pore size of porous media, based on the observed relaxation times of fluid within the pore space [5, 8-13]. It is important to note that the relaxation time depends on the diffusion regime. In the fast diffusion regime, only the ground mode relaxation time can be detected and it is directly connected to the pore size, where $\frac{1}{T_2} = \rho_2 S/V$, with *S/V* representing the surface-to-volume ratio. However, if the fluid relaxation occurs outside the fast diffusion regime, the relaxation times are proportional to the square of the pore size. The difficulty in detecting non-ground modes has led to the fast-diffusion method being widely employed.

Many recent studies, however, have shown that fluid relaxation may occur in the intermediate regime [9-15]. Müller-Petke et al. [11] proposed an approach to determine the average pore size, stressing that relaxation may occur outside the fast diffusion regime. Afrough et al. [9, 10] emphasized the importance of nonground modes, successfully detecting these modes and using them to estimate the pore size and surface relaxivity of the employed porous systems. Our recent work [13] focused on the correlation between the relaxation time and the temperature-dependent fluid self-diffusion. We observed that the observed relaxation times change across a range of temperatures. Notable highlights of this method include simple temperature control and straightforward nonlinear fitting. These features make our new method both easy to implement and practical.

Within the intermediate regime of BT theory, relaxation times are inversely proportional to the fluid self-diffusion coefficient, which has a strong dependence on temperature. Both the diffusion-relaxation regime and the observed relaxation times experience shifts with temperature variation. These shifts when observed indicate that the fluid relaxation must be in the intermediate regime. Importantly, these shifts vary among different pore systems, due to their distinct petrophysical characteristics. In this work we shift the relaxation time for employed reservoir rock core plugs by changing sample temperatures in order to estimate the pore size and the surface relaxivity. Three pore geometrical models were utilized for sandstone core plugs, and the calculated pore sizes were compared with imaging methods, including scanning electron microscopy (SEM) and μCT [16]. The pore size distribution may be determined based on BT theory [7].

CPMG measurement was employed to detect the first non-ground mode for glass microcapillary model systems, and to explore the correlation between T_2 relaxation time and the temperature-dependent self-diffusion of fluid in sandstone core plugs. This work is based on three assumptions: 1, the estimated pore size is the dominant pore size; 2, the surface relaxivity is independent of temperature over the range of temperatures employed; 3, fluids are in a localization regime, meaning the fluid diffuses within the pores rather than between them [17, 18].

2 Theory

2.1. Brownstein-Tarr theory

Diffusion effects in MR can be elucidated with the Bloch-Torrey equations. Brownstein and Tarr provided a mathematical solution to the Bloch-Torrey equations. This approach ultimately leads to an ordinary diffusion or heat equation.

$$D\nabla^2 M(r,t) = \frac{\partial M(r,t)}{\partial t} \tag{1}$$

Where *D* is the fluid self-diffusion coefficient in the pore space, *M(r,t)* is the net magnetization.

With a Fourier boundary condition, Brownstein and Tarr found the multi-exponential MR decay

$$M(r,t) = M(0)\sum_{i=1}^{n} I_{2,n} e^{-\frac{t}{T_{2,n}}} \tag{2}$$

Where $I_{2,n}$ is the n-th relative intensity, $T_{2,n}$ is the transverse relaxation time; n=0 is the ground relaxation mode, and n>0 are non-ground relaxation modes.

Pore shape and size significantly influence the fluid relaxation process. Therefore, Brownstein and Tarr proposed three geometries (planar, cylindrical, and spherical) to represent the pore space. The solutions corresponding to each of these geometries are as follows:

(a) For the planar geometry:

$$I_{2,n} = 4\frac{\sin(\xi_{2,n})^2}{\xi_{2,n}[2\xi_{2,n}+\sin(\xi_{2,n})]} \tag{3}$$

$$T_{2,n} = \frac{a^2}{D{\xi_{2,n}}^2} \tag{4}$$

$$\xi_{2,n}\tan(\xi_{2,n}) = {\rho a}/{D} \tag{5}$$

(b) For the cylindrical geometry:

$$I_{2,n} = \frac{4\,J_1^2(\xi_{2,n})}{{\xi_{2,n}}^2[J_0^2(\xi_{2,n})+J_1^2(\xi_{2,n})]} \tag{6}$$

$$T_{2,n} = \frac{a^2}{D{\xi_{2,n}}^2} \tag{7}$$

$$\xi_{2,n}\frac{J_1(\xi_{2,n})}{J_0(\xi_{2,n})} = {\rho a}/{D} \tag{8}$$

(c) For the spherical geometry:

$$I_{2,n} = \frac{12[\sin(\xi_{2,n})-\xi_{2,n}\cos(\xi_{2,n})]^2}{{\xi_{2,n}}^3[2\xi_{2,n}-\sin(\xi_{2,n})]} \tag{9}$$

$$T_{2,n} = \frac{a^2}{D{\xi_{2,n}}^2} \quad (10)$$

$$1 - \xi_{2,n}\cot(\xi_{2,n}) = {\rho a}/{D} \quad (11)$$

where a is the pore size; ρ is the surface relaxivity; D is the self-diffusion coefficient; The $\xi_{2,n}$ are the positive roots of the characteristic Eqs. (5), (8), and (11).

The diffusion regime is defined by the BT number, represented as $\rho a/D$. When $\rho a/D < 0.1$, relaxation is within the fast diffusion regime [19]. In this regime, the fluid relaxation is uniform and the MR behavior exhibits an exponential decay. However, in the case where $\rho a/D \sim 1$ or $\rho a/D >> 1$, the fluid relaxation occurs within the intermediate or slow diffusion regimes. Within these regimes, the MR decay is multi-exponential, even for a single pore size, but it is dominated by the ground mode.

2.2 Direct measurement of pore size and surface relaxivity

In this section, we employ our new method to estimate the pore size and surface relaxivity for porous media [13]. The correlation between temperature and relaxation behavior was utilized. The proposed method was employed to measure three sandstone samples. Three pore geometries were utilized for analysis, with three different nonlinear fitting equations.

By integrating the characteristic Eqs. (5), (8), (11) and relaxation time equation (4) yields the distinct equations for planar, cylindrical, and spherical pore geometries:

$$\rho_2\sqrt{\frac{T_{20}}{D}} = \tan\left(\frac{a}{\sqrt{T_{20}D}}\right) \quad (12)$$

$$\frac{\rho_2}{D} = \frac{1}{\sqrt{T_{20}D}}\frac{J_1\left(\frac{a}{\sqrt{T_{20}D}}\right)}{J_0\left(\frac{a}{\sqrt{T_{20}D}}\right)} \quad (13)$$

$$\frac{\rho_2 a}{D} = 1 - \frac{a}{\sqrt{T_{20}D}}\cot\left(\frac{a}{\sqrt{T_{20}D}}\right) \quad (14)$$

For spherical and cylindrical geometries, we defined the same variables y_1 and x:

$$y_1 = 1/D \quad (15)$$

$$x = \sqrt{T_{20}D} \quad (16)$$

Therefore, the nonlinear fitting equations for spherical and cylindrical geometries were:

$$y_1 = \frac{1}{\rho_2}\left[\frac{1}{a} - \frac{1}{x}\cot\left(\frac{a}{x}\right)\right] \quad (17)$$

$$y_1 = \frac{1}{\rho_2 x}\frac{J_1\left(\frac{a}{x}\right)}{J_0\left(\frac{a}{x}\right)} \quad (18)$$

In the case of the planar geometry, we defined y_2 and retain the same variable x as in Eq. (16):

$$y_2 = \sqrt{\frac{T_{20}}{D}} \quad (19)$$

Combining y_2 with x changes Eq. (20), enabling the determination of the nonlinear fitting equation for the planar geometry:

$$y_2 = \frac{1}{\rho_2}\tan\left(\frac{a}{x}\right) \quad (20)$$

The three nonlinear fitting equations (17), (18), and (20) were utilized to determine the pore size and surface relaxivity for the sandstone samples.

3 Experimental

In our work to detect the first non-ground mode and to validate BT theory, we utilized three glass microcapillary samples (Borosilicate glass, VitroCom, New Jersey, USA). We conducted experiments with three planar glass microslides, Glass-I, Glass-II, and Glass-III, with slit sizes of 100 μm, 50 μm, 30μm. Additionally, a cylindrical microcapillary, Glass-IV, with a diameter of 100 μm, was employed. Fig. 1 shows the dimensions of the four glass microcapillaries. Given the small volume of the pore space, multiple pieces were required for MR measurement to achieve a satisfactory SNR. Accordingly, 10, 35, 60, and 30 pieces were employed for Glass-I, Glass-II, Glass-III, and Glass-IV measurements, respectively.

CPMG experiments with the glass microcapillaries were carried out on a 4.7 T vertical-bore superconducting magnet (Cryomagnetics, Inc., Oak Ridge, TN) paired with a Redstone NMR spectrometer console (Tecmag, TX, USA). The sample vial was positioned within the sensitive region of a Doty DSI-874 ^{1}H RF probe (Doty Scientific, Inc., Columbia, SC), with a dead time of 6 μs. Radio frequency excitation was conducted with the RF probe, driven by a 300 W M3205A pulse amplifier (American Microwave Technology, Inc., Brea, CA). The 90° pulse duration was 24 μs. The echo spacing was 500 μs, with 8192 echoes. For all glass microcapillary samples, the repeat delay was 20 seconds, with a total of 128 scans. The total experimental duration for each microcapillary sample was approximately 0.8 hours. These measurements were conducted at ambient

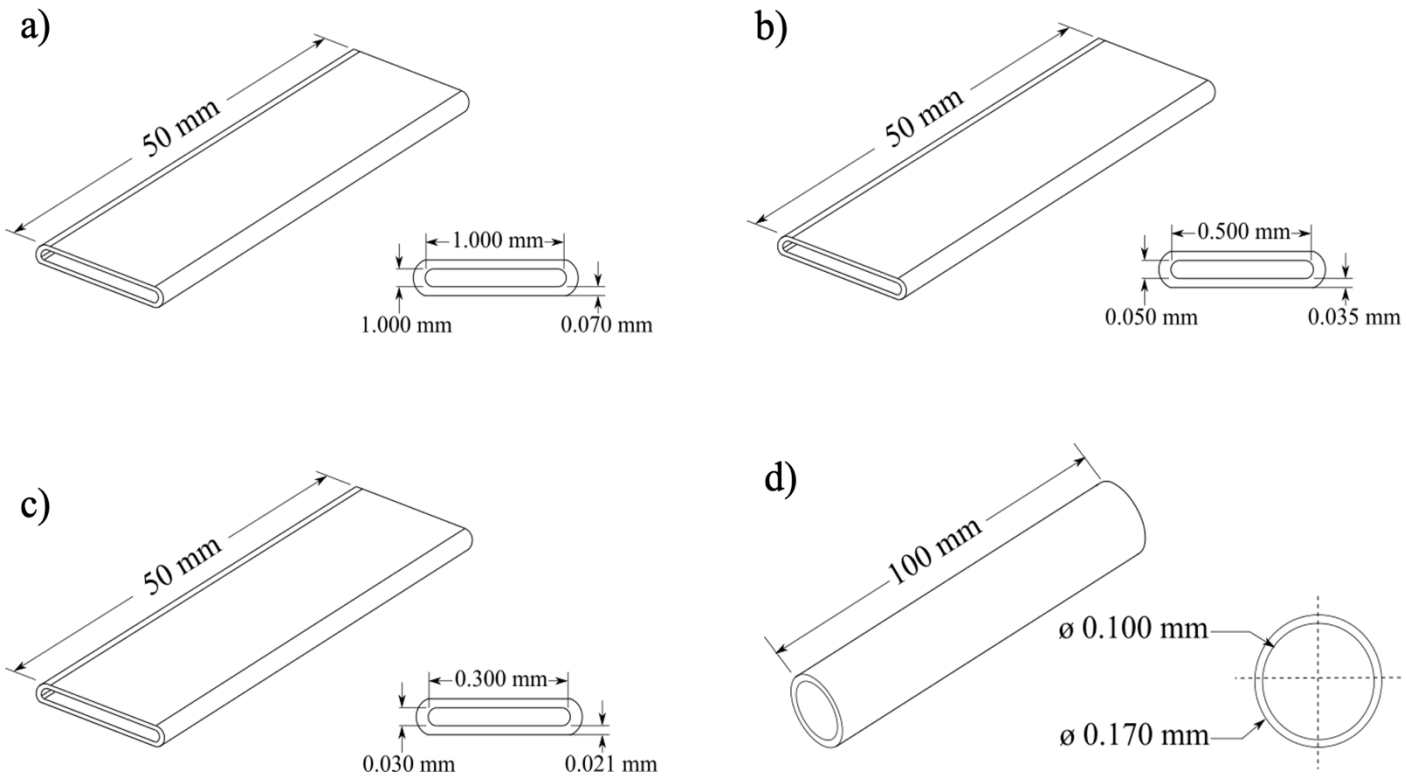

Fig. 1. Schematic diagram of the Glass-I (a), Glass-II (b), Glass-III (c), and Glass-IV (d) samples. The Glass-I, Glass-II, and Glass-III samples have the same length of 50 mm, while they differ in the width and slit size. The widths are 1 mm, 0.5 mm, and 0.3 mm, for Glass-I, Glass-II, and Glass-III, respectively. The slit sizes (pore sizes) are 0.1 mm, 0.05 mm, and 0.03 mm for Glass-I, Glass-II, and Glass-III, respectively. The Glass-IV sample (d) has a length of 100 mm and a diameter of 0.1 mm.

temperature, and no temperature control was implemented.

Sandstone samples of Berea, Buff Berea, and Nugget were obtained from Kokurek Industries (Caldwell, Texas, USA) and cut into cylindrical core plugs with a diameter of 25 mm and a length of 50 mm. The sandstone samples were saturated with a 2% (w/v) *NaCl* brine solution.

CPMG experiments for sandstone samples were conducted with a 8.5 MHz Maran DRX-HF instrument (Oxford Instruments, Abingdon, UK). The 90° pulse duration was set at 10.5 μs, with an echo spacing of 200 μs. The short echo time employed minimizes the effect of diffusion through internal magnetic field gradients. The number of echoes was set at 2048 for Berea, Buff Berea, and Nugget. For Berea, Buff Berea, and Nugget, the number of scans was 8 with a 3-second repeat delay, resulting in a total measurement time of 24 seconds at each temperature. The signal to noise ratio (SNR) was greater than 200 for Berea, and Buff Berea sandstones, and greater than 100 for the Nugget sandstone.

In this work, we utilized sample temperatures of 5 °C, 15 °C, 25 °C, 35 °C, and 45 °C. These temperatures were maintained with a thermal DryBath (HC110-pro, Scilogex, Hartford Country, CT, US). The DryBath approach to temperature control was advantageous since temperature control was primarily by conduction from the metal block surrounding the core plug samples. The DryBath was used to temperature control multiple samples simultaneously. We calculated the necessary heating or cooling time for each desired temperature by solving the heat conduction equation. For this work, we employed 30 minutes for the largest temperature difference of 20 degrees. CPMG measurement was rapid so we assume the sample temperature is the pre-equilibrated temperature of the DryBath. We assumed that the diffusion coefficient of the brine solution is approximately equivalent to the diffusion coefficient of water. The self-diffusion coefficient of water was $1.32*10^{-9}$ m^2/s, $1.76*10^{-9}$ m^2/s, $2.30*10^{-9}$ m^2/s, $2.90*10^{-9}$ m^2/s, and $3.6*10^{-9}$ m^2/s at the temperatures employed. These values were obtained by quadratic fitting to experimental results in references [21-25].

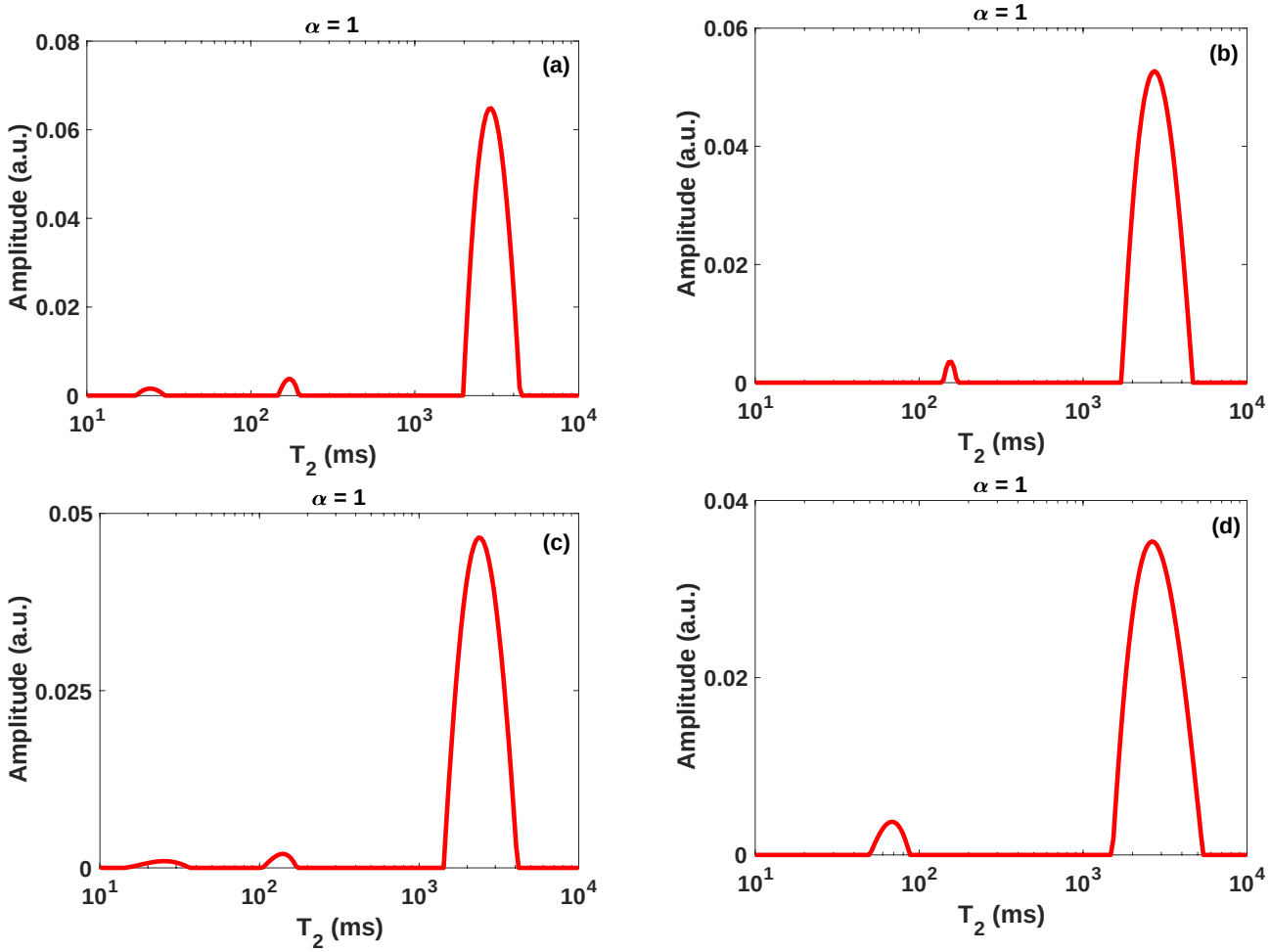

Fig. 2. (a)-(d) T_2 distributions of Glass-I, II, III, and IV samples. The dominant peak in T_2 distribution represents the ground mode relaxation time distribution from the three glass samples. Non-ground modes were observed in all samples.

4 Results and discussion

4.1 Glass microcapillaries

To identify the non-ground modes and assess BT theory, we conducted CPMG measurements with Glass-I, II, III, and IV samples. The T_2 distribution of the CPMG decay data was determined with the Butler-Reeds-Dawson (BRD) method. Fig. 2 (a-d) shows the T_2 distribution for the four glass samples.

Fig. 2 (a) shows the T_2 distribution of the Glass-I sample, which includes three peaks. The two small peaks are located at 168 ms and 24 ms. The known pore size, along with these two T_2 times, allows for the calculation of the parameters $\xi_{2,1}$ and $\xi_{2,2}$ based on Eq. 4. Upon determining these $\xi_{2,n}$ parameters, we can proceed to calculate the surface relaxivities, using Eq. 5, which are found to be 68 *μm/s* and 69 *μm/s*. This proves that the two small peaks represent non-ground modes originating from a single pore size. In addition the existence of these peaks in the T_2 distributions measured in these model systems confirms the correctness of BT theory for analogous inorganic porous media. The pore shape of the glass microslide samples was obviously planar. For the Glass-II sample, the T_2 distribution, shown in Fig. 2 (b), exhibits a dominant peak along with one smaller peak, which is the first non-ground mode. The first non-ground mode relaxation time is 157 *ms*. Fig. 2 (c) shows the T_2 distribution of the Glass-III sample. The first and second non-ground modes were observed at 150 *ms* and 20 *ms*, respectively.

Fig. 2 (d) shows the T_2 distribution from water filled 100 *μm* glass microcapillaries with a cylindrical pore geometry. This distribution features a dominant peak accompanied by a smaller peak, which is the first non-ground mode. The amplitude of the first non-ground mode for the Glass-IV sample is significantly higher than those observed in the planar glass microslide samples. The first non-ground relaxation time was measured to be 68 *ms*. Knowing the pore size and observed T_{21} time, the surface relaxivity of Glass-IV sample was estimated to be 76 *μm/s*. This value is quite close to the 68 *μm/s* from the Glass-I sample. The same glass material should have comparable surface relaxivities.

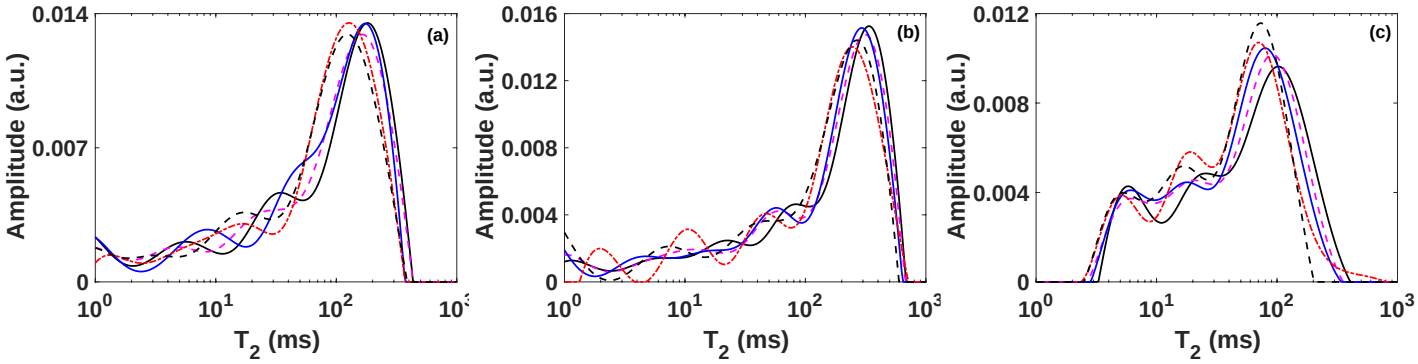

Fig. 3. (a)-(c) T_2 distributions of Berea, Buff Berea, and Nugget sandstones at variable temperature: 5 °C (——), 15 °C (---), 25 °C (——), 35 °C (—.), and 45 °C (---). The shift in the T_2 distribution is clearly observed.

The fast diffusion assumption permits the direct conversion of the T_2 distribution to the pore size distribution. However, if applied to Glass-I to Glass-IV samples, this approach would result in erroneous peaks in a pore size distribution. This conflicts with the single pore size of the model systems utilized. This discrepancy is particularly noticeable for the Glass-IV sample, where the first non-ground modes could easily be misinterpreted as signal emanating from small pores.

Based on the calculated surface relaxivities and the known pore sizes, the BT numbers for the four samples were calculated as 1.5, 0.75, 0.5, and 1.65. As the pore size decreased from Glass-I to Glass-III, the calculated BT numbers suggest a shift of the fluid relaxation regime towards fast diffusion. BT theory predicts that decreasing the BT number will reduce the amplitude of the non-ground modes. The decrease in amplitude of non-ground modes is not clearly visible in the displayed T2 distributions, but a decrease is observed when calculating the area under the curve of the first non-ground mode distributions.

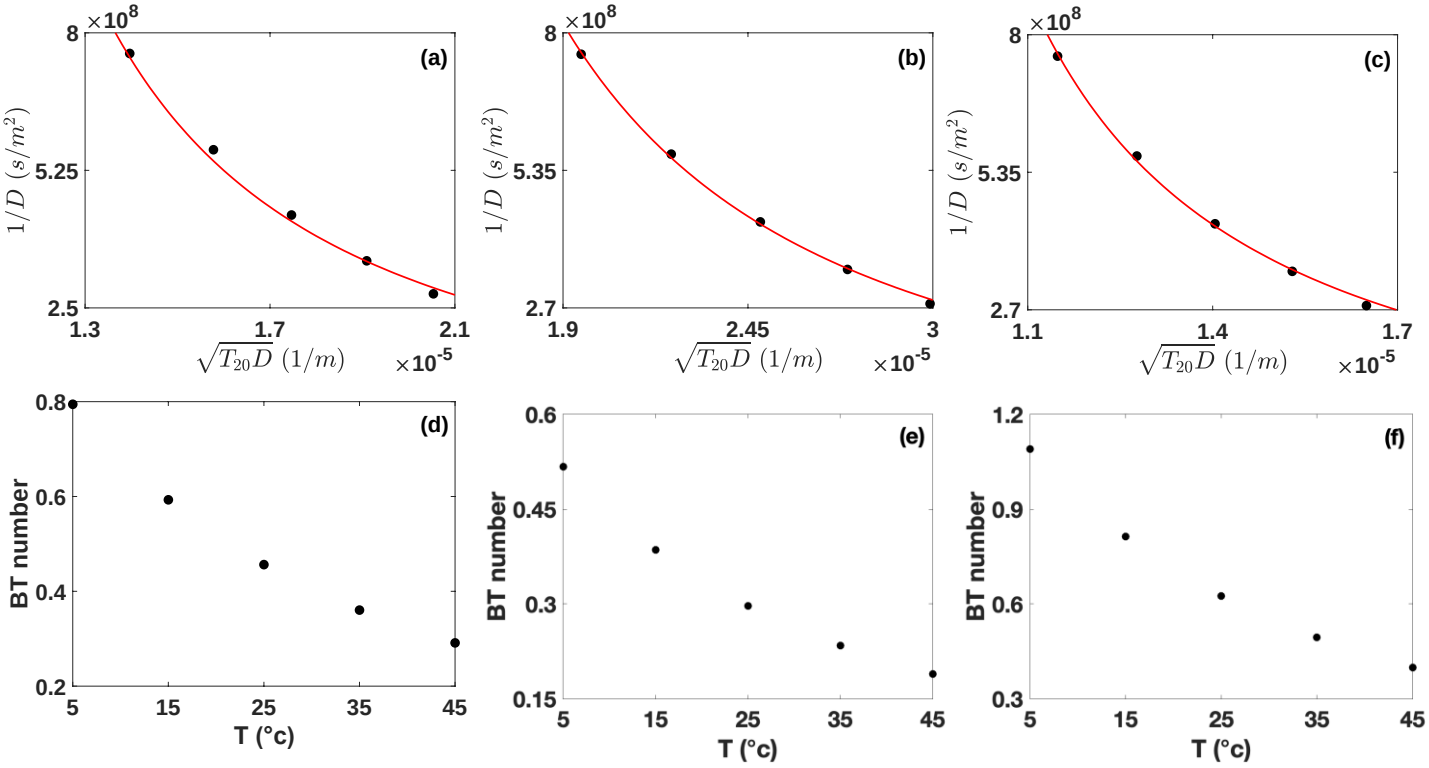

Fig. 4. (a)-(c) Nonlinear fitting of experimental results with Berea, Buff Berea, and Nugget sandstones. (.) is the experiment result and (-) is the nonlinear fitting result with a spherical pore geometry. (d)-(f) The BT number of the three sandstones with variable temperature. The BT number decreases as the temperature increases. Th BT number shows the three sandstones are in the intermediate regime.

Table 1. Pore size and surface relaxivity for Berea, Buff Berea, and Nugget sandstones. Independent pore size estimates from imaging methods are included.

Sandstone	Pore size (μm)			SEM (3D) (μm)	μCT (μm)	Surface relaxivity ($\mu m/s$)		
	Spherical	Cylindrical	Planar			Spherical	Cylindrical	Planar
Berea	26	20	25	26	22	80	63	117
Buff Berea	37	32	35	44	36	45	42	64
Nugget	25	34	24	42	42	101	104	176

4.2 Sandstone

CPMG measurements were performed on sandstone samples, Berea, Buff Berea, and Nugget at variable temperature. The T_2 distributions of these three sandstone samples are shown in Fig. 3 (a-c). The T_2 distributions of Berea and Buff Berea consist of one dominant peak along with a series of smaller peaks, while that for the Nugget sandstone exhibits one dominant peak and two smaller peaks.

This work focuses on the dominant pore size, which corresponds to the MR signal at the peak of the T_2 distribution. The peak of the T_2 distribution is the ground mode relaxation time of large pores within the examined pore systems. The shifts in the peak of the T_2 distributions is clearly observed in Fig. 3 (a-c). It confirms that the sandstone samples are in the intermediate regime. The relaxation time would be unchanged, as temperature changed, if the fluid relaxation occurred in the fast diffusion regime. This assumes the surface relaxivity is temperature independent. The observed relaxation times of the dominant peak T_2 distributions across five temperatures were utilized to estimate the pore size and surface relaxivity of Berea, Buff Berea, and Nugget sandstones. All three geometrical models derived from BT theory were applied to estimate pore size and surface relaxivity. The nonlinear fitting equations were discussed earlier. Fig. 4 (a)-(c) show the nonlinear fittings with a spherical pore geometry for Berea, Buff Berea, and Nugget, respectively. The variations of BT number with temperature are depicted in Fig. 4 (d)-(f). Based on the lowest BT number of 0.17, the sandstones examined in this work are in the intermediate regime.

Table 1 shows the estimated dominant pore size and surface relaxivity for the three sandstones, along with the pore size determined from SEM and μCT. The dominant pore size estimate for Berea was 26 μm, 20 μm, and 25 μm, corresponding to the spherical, cylindrical, and planar geometries, respectively. These estimations align well with the 26 μm obtained from SEM measurement and 22 μm derived from μCT measurement. The surface relaxivities calculated with the three geometrical models were 80, 63, and 117 $\mu m/s$ for the Berea sample. For Buff Berea sandstone the estimated pore size was 37 μm with a spherical geometry, 32 μm with a cylindrical geometry, and 35 μm with a planar geometry. These results are in close agreement with the μCT method of 36 μm, while they are slightly smaller than the SEM method of 44 μm. The surface relaxivity of Buff Berea, calculated using the three geometries, was determined to be 45, 42, and 64 $\mu m/s$ for spherical, cylindrical, and planar models. In the case of Nugget sandstone, the shape of the pore may influence the pore size estimates. The calculated pore size of 34 μm with a cylindrical geometry aligns with the measurements from imaging methods. However, the pore size estimates of 25 and 24 μm with the spherical and planar geometries, differ from the imaging methods. This may suggest that the pores in Nugget sandstone are more likely to exhibit a cylindrical shape. It is widely recognized that paramagnetic material on the pore surface significantly affects the surface relaxation. The surface relaxivity is anticipated to scale with the amount of paramagnetic material. Nugget sandstone, with a discernible red color, suggests a substantial presence of paramagnetic substances. As a result, the surface relaxivity of Nugget sandstone is higher than that of Berea and Buff Berea sandstones. The calculated surface relaxibity of Nugget with three geometries were 101, 104, 107 $\mu m/s$.

Fig. 4 (d-f) shows the variation in the BT number with temperature. These figures clearly show that fluid relaxation within the sandstones moves towards the fast diffusion regime as we increase temperature. The fluid relaxation would move into the fast diffusion regime if we increased the fluid temperature to 70 or 80 degrees for these samples. In such a case, the fluid self-diffusion would no longer impact the MR relaxation times, resulting in a direct relationship between the pore size and the relaxation time.

4.3 Pore size distribution determination of sandstone

The pore size distribution is a critical parameter in petrophysics and core analysis. The results described above show how we may determine the surface relaxivity and non-ground modes of relaxation. The MR signal decay in the intermediate regime results in an individual pore size contributing to the first non-ground mode signal at a shorter lifetime. This signal could be interpreted as originating from smaller pores, based on the fast diffusion assumption. Our recent work has been aimed at resolving this discrepancy [7]. Outside of the fast diffusion regime, the observed shorter relaxation times could potentially result from a combination of T_{20} lifetime of small pores (T_{20_S}) and T_{21} lifetime of large pores (T_{21_L}). In this study, we sought to convert the T_{20} distribution to the pore size distribution. Long experimental T_2 times can be regarded as the T_{20} times of the large pores (T_{20_L}) neglecting bulk relaxation. However, determining the T_{20_S} becomes

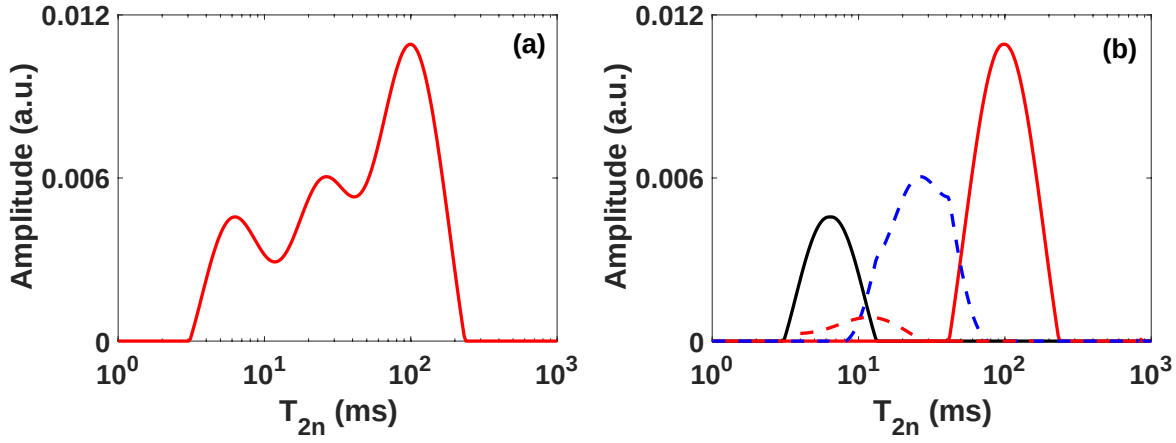

Fig. 5. (a) (-) is the experimental T_2 distribution of Nugget sandstone. (b) (-) is the T_2 distribution of larger pores, (-) and (----) are the T_2 distribution of small pores ; (---) is the calculated first non-ground T_{21} distribution of the larger pores.

challenging due to the overlap between the T_{20_S} and T_{21_L}. Determination of T_{20_S} requires the subtraction of T_{21_L}, in cases when they are overlap.

In section 4.2, we reported the surface relaxivities for our measured sandstones. With knowledge of the T_{20_L}, surface relaxivity, and the diffusion coefficient of fluid, we can determine the parameter of $\xi_{2,0}$, and consequently the first non-ground mode of larger pores (T_{21_L}). We then calculated the first non-ground mode T_{21} distribution for larger pores, and subtracted this from the observed T_2 distribution. This enabled us to determine the entire T_{20} distribution for the sample being studied. Following BT theory, we transformed the T_{20} distribution into a pore size distribution.

In this work we assume the pore size distribution dominates the width of the T_2 distribution. We need to ensure the regularization parameter α does not dominate the width of the peaks in the distributions. A smaller α, such as α <0.1, results in a narrow T_2 distribution. A large α, such as α=100, will blur the T_2 distribution and overwhelms discrimination of the ground and first nonground modes. In this work, we employed α=1 for the inversion of the T_2 distribution because it facilitates the detection of non-ground modes. Testing shows this α does not artificially increase the width of the experimental distribution.

In this work, we estimated the pore size distribution of the Nugget, Berea, and Buff Berea sandstones. Fig. 5 (a) shows the observed T_2 distribution of the Nugget sample. Using the symmetry of the distribution, we decomposed it into three independent peaks, as shown in Fig. 5 (b). These independent peaks suggest that the Nugget sandstone is characterized by three dominant pore sizes, large, medium, and small. Applying BT theory, we calculated the T_{21} distribution of large pores. This distribution is located at the T_2 times contributed by the medium and small pores. The subtraction of this component allows for an accurate determination of the proportion of medium and small pores in the sample.

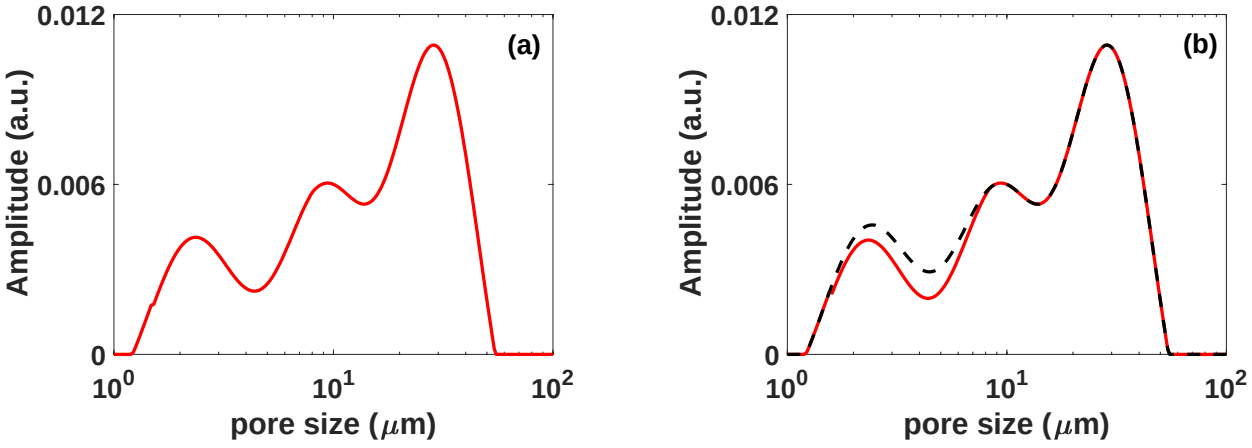

Fig. 6. (a) (-) the determined pore size distribution of Nugget sandstone. (b) (-) and (---) are pore size distributions with and without the substraction of the first non-ground mode of larger pores.

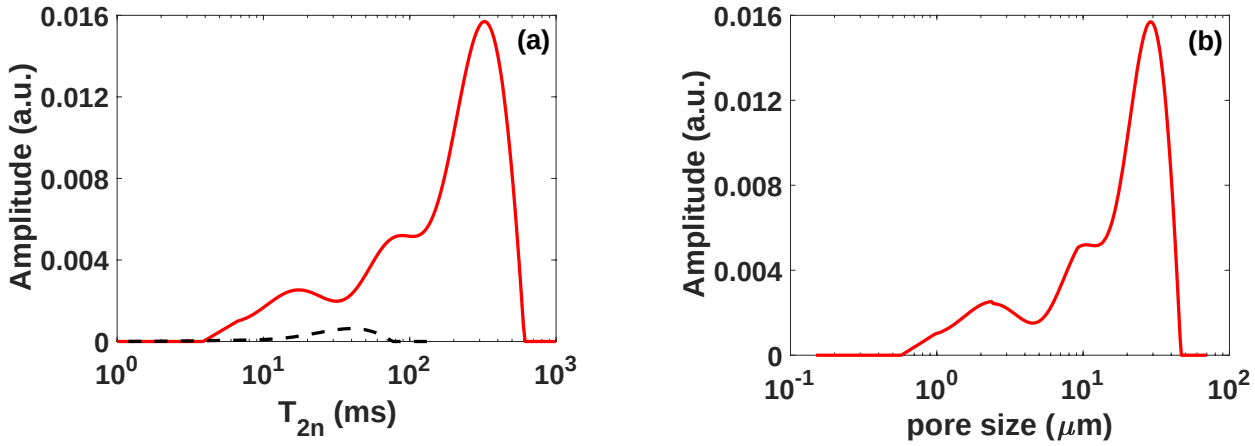

Fig. 7. (a) (-) the T_2 distribution of Buff Berea sandstone, (---) the calculated first non-ground T_{21} distribution of larger pores. (b) (-) the calculated pore size distribution of Buff Berea sandstone.

By removing the T_{21} distribution of larger pores, we were able to determine the T_{20} distribution for Nugget sandstone. This T_{20} distribution was then converted into the pore size distribution, as shown in Fig. 6 (a). Fig. 6 (b) shows two pore size distribution, one with and another without the subtraction of the first non-ground mode of large pores. The difference shows the impact of the first non-ground mode of large pores on the experimental pore size distribution.

It is worth noting that the BT number controls the amplitude of the first non-ground mode of the employed sample. The first non-ground mode of Nugget sandstone is large enough to merit attention. In the case of the Nugget sandstone employed, with a BT number of 0.7 at 25 °C, the area of the first non-ground mode is approximately 10 % of the ground mode. In samples with higher BT numbers, the proportion of the first non-ground mode will be more significant. If the BT number were 1.5 or even 2, the first non-ground mode area would be 20 % or 30 % of the ground mode. However, for samples with lower BT numbers, the amplitude of the first non-ground mode will likely be less than 10%, thus, its influence on the pore size distribution becomes less significant. In this study, BT numbers of the Buff Berea and Berea sandstone at 25 °C were 0.45 and 0.3, respectively. These lower BT numbers mean the relaxation behavior of the employed samples is closer to the fast diffusion regime, suggesting a smaller amplitude of the first non-ground mode. Fig. 7 (a) shows the observed T_2 distribution alongside the calculated T_{21} distribution of larger pores. The amplitude of the first non-ground mode is approximately half that of the third peak of the T_2 distribution. This suggest that its presence will influence the proportion of small pore sizes, specifically around the pore size of 5 *um*. Fig. 7 (b) shows the pore size distribution of Buff Berea sandstone after removing the influence from the first non-ground mode of larger pores. Fig. 8 (a) shows the observed T_2 distribution of the Berea sample accompanied by the calculated first non-ground mode distribution of larger pores. The determined pore size distribution is shown in Fig. 8 (b). It should be note that the T_2 distributions utilized in Figs.

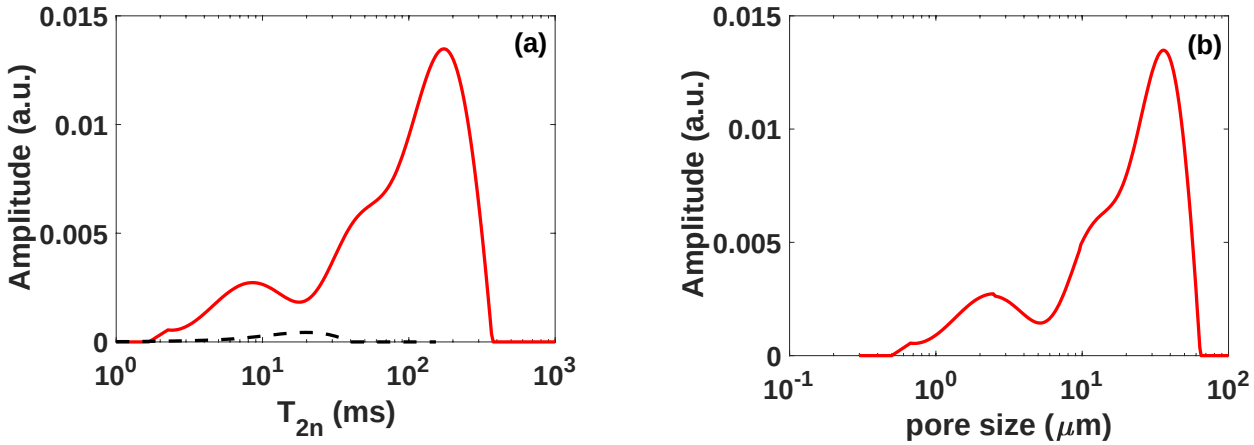

Fig. 8. (a) (-) the T_2 distribution of Berea sandstone, (---) the calculated first non-ground T_{21} distribution of larger pores. (b) (-) the calculated pore size distribution of Berea sandstone.

7(a) and 8 (a) originate from Fig. 3. The distribution used in Figs. 7 and 8 has a zero amplitude in the short lifetime limit.

In this section, we described the method for determining the pore size distribution based on BT theory, using three sandstone samples for illustration. We calculated the first non-ground mode of larger pores based on BT theory, and discussed the necessity of its subtraction for determination of pore size distributions, with the BT number. A comparison of pore size distributions with direct imaging work is an effective tool to validate the method developed in this study. Incorporation of such a comparison will be considered in future work.

5 Conclusion

Determinations of pore size and pore size distribution are fundamental to core analysis. The MR relaxation time is commonly employed for this purpose, based on an assumption of fast diffusion. However, this assumption is not universally true, especially for samples with larger pore sizes or higher surface relaxivity. In this study, we follow BT theory, emphasizing the intermediate regime to estimate both pore size and surface relaxivity for sandstone core plugs.

Glass microcapillaries served as an ideal model system to validate BT theory. A fixed and known pore sizes, and pore geometry, makes the glass microslides a superior system for control measurements. We were able to detect non-ground modes, and by changing the microslide pore size, the observed shift in relaxation times was found to align with predictions made by BT theory.

MR signal decay from fluids within the pore space is influenced by factors including the pore size, the surface relaxivity and fluid self-coefficient, as described by BT theory. In this work, we employed the correlation between the temperature-dependent self-diffusion coefficient of the fluid and its relaxation behavior within the pore space, to estimate the pore size and surface relaxivity. By changing the fluid self-diffusion coefficient with temperature, we observed shifts in both the diffusion regime and the relaxation times of the sample. The amplitude of the shift depends on the distinct properties of the sample being examined. We utilized this shift to estimate the pore size and surface relaxivity of sandstone samples, with a nonlinear fitting approach. Three nonlinear fitting equations were derived, based on the three pore geometrical models of BT theory. Sandstones were employed to test our proposed method. The determined pore sizes align well with direct imaging methods. The calculated BT numbers indicate that all samples utilized in this work are within the intermediate regime.

In this paper, we have validated and applied BT theory to sandstone reservoir rock core plugs. The correlation between relaxation time and temperature underscored the importance of the intermediate regime. The fast diffusion regime is not universal for core plug systems.

We thank the Natural Sciences and Engineering Research Council of Canada (NSERC) for a Discovery grant [2022-04003] and an Alliance grant [571885-21]. We thank TotalEnergies and Green Imaging Technologies for financial support. Bruce J. Balcom acknowledges the Canada Research Chairs Program for a Research Chair in Materials Science Magnetic Resonance Imaging [950-230894]. We thank Dr. Andy Sederman of the University of Cambridge for suggesting the glass microcapillary model system. We thank Isobel Jager for assistance with the figures.

References

1. R.J.S. Browns, R. Fatt, Trans Amer Inst Min and Met Eng, **207** (1956)
2. R. L. Kleinberg, *Experimental methods in the physical sciences* (Academic Press, San Diego, 1999)
3. K. Brownstein, C. Tarr, Phys. Rev. A, **16** (1979)
4. G. Coates, L. Z. Xiao, M. Prammer, *NMR logging: Principles and Applications* (Halliburton Energy Services, Houston, 1999)
5. Y. Q. Song, Phys. Rev. Lett., **85** (2000)
6. H. C. Torrey, Phys. Rev., **104** (1956)
7. P.Y. Yan, J.F. Guo, F. Marica, B.J. Balcom, Geoenergy Science and Engineering, (Accepted pending minor revisions)
8. Y. Q. Song, S. Ryu, Nature, **406** (2000)
9. A. Afrough, S. Vashaee, L. Romero-Zeron, B.J. Balcom, Phys. Rev. Appl., **11** (2019)
10. A. Afrough, F. Marica, B. MacMillan, B. J. Balcom, Phys. Rev. Appl, **16** (2021)
11. M. Muller-Petke, R. Dlugosch, J. Lehmann-Horn, Geophysics, **80 (**2015)
12. H. B. Liu, M. N. d'Eurydice, S. Obruchkov, P. Galvosas, J Mag Reson, **246** (2014)
13. P.Y. Yan, F. Marica, J.F. Guo, B.J. Balcom, Phys. Rev. Appl., **20** (2023)
14. E. Lucas Oliveira, A. G. Araujo Ferreira, W. A. Trevizana, C. A. Fortulan, T. J. Bonagamba, J Magn Reson, **292** (2018)
15. E. Lucas-Oliveira, A. G. Araujo-Ferreira, W. A. Trevizana, B. C. C. dos Santos, T. J. Bonagamba, J. Petrol. Sci. Eng., **193** (2020)
16. H. Safari, B. J. Balcom, and A. Afrough, Comput. Geosci., **156** (2021)
17. R. L. Kleinberg, Magn. Reson. Imaging, **12** (1994)
18. M. D. H¨urlimann, J. Magn. Reson., **131** (1998)
19. S. Ryu, SPWLA 50th Annual Logging Symposium (2009)
20. K. Keating, Near Surf. Geophys., **12 (**2014)
21. R. Mills, J. Phys. Chem., **77** (1973)
22. A. J. Easteal, W. E. Price, L. A. Woolf, J. Cliem. Soc., Faraday Trans. I, **76** (1989)
23. P. S. Tofts, D. Lloyd, C. A. Clark, G. J. Barker, G. J. M. Parker, P. McConville, C. Baldock, J. M. Pope, Magn. Reson. Med, **43** (2000)
24. M. Holz, S. R. Heil, A. Sacco, Phys. Chem. Chem. Phys, **2** (1000)
25. T. L. Chenevert, C. J. Galb´an, M. K. Ivancevic, S. E. Rohrer, F. J. Londy, T. C. Kwee, C. R. Meyer, T. D. Johnson, A. Rehemtulla, B.D. Ross, J. Magn. Reson.Imaging, **34** (2001)